Received: 15 March 2019

Revised: 6 May 2019

Accepted article published: 27 May 2019

Published online in Wiley Online Library: 12 June 2019

(wileyonlinelibrary.com) DOI 10.1002/pi.5860

Morphology and ionic conductivity relationship in silk/cellulose biocomposites

Bailey Blessing,^a Cory Trout,^b Abneris Morales,^a Karleena Rybacki,^d Stacy A Love,^d Guillaume Lamoureux,^{a,d} Sean M O'Malley,^{b,d} Xiao Hu^c and David Salas-de la Cruz^{a,d*}

Abstract

The relationship between morphology and the ionic conductivity of polysaccharide–protein bio-electrolyte membranes is explored in this study. Structural proteins and polysaccharides form hydrophobic and electrostatic interactions, and the resulting matrices can exhibit novel and useful properties. However, transforming these natural biomacromolecules from their native state to a more usable form is challenging. The structural, morphological, thermal, mechanical and electrical properties of biomaterials composed of microcrystalline cellulose and *Bombyx mori* silk when regenerated together using ionic liquids and various coagulation agents were investigated using a diverse set of techniques including Fourier transform infrared spectroscopy, SEM, TGA, DSC, X-ray scattering, AFM-based nanoindentation and dielectric relaxation spectroscopy. The surface topography of the films reveals morphological changes with varying coagulation agents and ionic liquids. It was found that the thermal and mechanical properties were dependent on intermolecular interactions dictated by the type of ionic liquid used during the coagulation process. X-ray scattering provided information on how the cellulose crystallinity varied with coagulation agent. Specifically, samples coagulated with hydrogen peroxide showed an increase in cellulose crystallinity impacting properties such as elasticity, hardness and ionic conductivity of the biocomposites. In addition, the results revealed a strong correlation between β -sheet content and ionic conductivity and cellulose crystallinity. The results provided evidence that the ionic conductivity is dependent on protein β -sheet content and cellulose crystallinity.

Keywords: cellulose; silk; morphology; ionic conductivity; β -sheets; X-ray scattering

INTRODUCTION

Recently, biomaterials have become of great importance in material sciences, medicine and bioengineering. The interest in this class of materials stems from its numerous advantageous properties that include abundance, biocompatibility, low cost, and tunable physical and morphological properties. 1,2 These materials have been used to create scaffolds for tissue growth as well as capsules used for drug delivery systems.² Creating implantable batteries using natural biomaterials has become significant in various medical applications.³ Having the ability to control the properties of these biomaterial-based batteries, including morphological, thermal and mechanical properties, is essential in creating devices which are minimally harmful in the human body and are advantageous in the medical field. In previous studies, it has been shown that the morphology of biocomposites can be changed as a function of ionic liquid and composition.⁴⁻⁶ This is important because it can induce changes in physicochemical properties of the natural-based material, which can lead to specificity in application.

Biocomposites from a mixture of proteins and polysaccharides are ideal for creating bio-electrolyte membranes which can exhibit high biocompatibility in the human body and adjustable ionic conductivity. One such protein includes *Bombyx mori* silk fibroin. It is produced by *Bombyx mori* silkworms in the form of fibers coated with sericin proteins with a repeat unit of [GAGAGS]_n and properties which include high toughness and tensile strength.⁷

Within this protein, there are crystalline structures which can include β -sheet secondary structures. These secondary structures can be deliberately changed from α -helices or random coils to β -sheets when using alcohol-based solutions.^{7,8}

Among the materials used to form a composite with silk are polysaccharides such as cellulose. The *Bombyx mori* silk has key amino acids with functional groups that are eligible to form hydrogen bonding with hydroxyl groups in microcrystalline Avicel cellulose. Cellulose is a natural biopolymer found in numerous sources including plants, generally in the form of cellulose I and more rarely found (or regenerated) as cellulose II with anti-parallel sheets. 9,10 Within cellulose, there is a complex hydrogen bonding network with intermolecular and intramolecular hydrogen bonds. 11,12 The short-distance chain packing and stiffness of cellulose, partially

- * Correspondence to: D Salas-de la Cruz, Department of Chemistry, Rutgers University, Camden, NJ, USA. E-mail: david.salas@camden.rutgers.edu
- a Department of Chemistry, Rutgers University, Camden, NJ, USA
- b Computational and Integrative Biology, Rutgers University, Camden, NJ, USA
- c Department of Physics and Astronomy, Department of Biomedical Engineering, Rowan University, Glassboro, NJ, USA
- d Center for Computational and Integrative Biology, Rutgers University, Camden, NJ, USA



from the complex hydrogen bonding network, make it challenging to break down and fully dissolve in common organic solvents or water.¹³ Instead, ionic liquids are used to complete the dissolution process for cellulose and silk.¹³ These ionic liquids have advantageous properties including a wide electrochemical window, good thermal stability and high ionic conductivity.14 The ionic liquid cation and anion associate with the oxygen and hydrogen of the cellulose hydroxyl groups, respectively, disturbing hydrogen bonding and causing dissolution. 13,15 Silk chains will undergo a similar process. In solution, cellulose and silk will interact through electrostatic, hydrogen bonding and hydrophobic-hydrophobic interactions.^{5,16} After the dissolution, a coagulation agent such as water, hydrogen peroxide or alcohol is added to wash out the ionic liquid. During this phase, the anions migrate from the biopolymer blend to the coagulant. Evidence for this is based upon the nearly complete absence of residual ionic liquid in the final blend as seen through different technical characterizations such as Fourier transform infrared spectroscopy (FTIR). As the anions are essential to keep the biomolecules separated, the polymer chains are able to aggregate in their absence. However, the coagulation agent rapidly replaces the anions once embedded in or next to the biopolymers, so that there is competition between coagulant molecules and other biopolymers in forming hydrogen bonds. This leads to phase separation with the formation of a hydrogel (biopolymer and water) and a liquid phase (water and ionic liquid).⁶ The final step consists of the removal of the coagulation agent and the formation of the intercalated protein-polysaccharide solid biocomposite. Combining the protein blend with polysaccharides helps to enhance physicochemical properties.5

When the materials are regenerated using different coagulation agents, the properties can vary in terms of morphological, thermal and mechanical properties. These differences can also lead to changes in ionic conductivity produced by a minimal amount of bound ionic liquid that remains in the films or by the retention of water molecules in the matrix after coagulation and drying. Two mechanisms, ion dissociation and ion diffusion, directly affect the ionic conductivity of homogeneous solid polymer electrolytes. It is possible to calculate the ion diffusion process by the Vogel–Fulcher–Tammann equation and the ion dissociation process by the Arrhenius equation. The equation

$$\sigma = q\rho_{\infty}\mu_{\infty} \exp\left(-\frac{E_{a}}{\overline{R}T}\right) \exp\left[-\frac{B}{\overline{R}(T - T_{0})}\right]$$
(1)

gives the ionic conductivity, 18 where q is the charge of the ions, ρ_{∞} is the total ion density, μ_{∞} is ion mobility, \textit{E}_{a} is the activation energy, T is the temperature, \overline{R} is the universal gas constant, B is an energy barrier constant and T_0 is the Vogel temperature. ^{17–19} The ion diffusion process also includes the hopping of ions as well as the segmental motion of polymer chains. 19-21 All of these processes are related to the morphology of the solid material, which can be partially expressed by the energy constant B in Eqn (1). According to the equation $B = B_{seq} + B_h$, B can be written in terms of two contributions: B_h , the energy barrier of ion hopping, and B_{seq} , the energy barrier for segmental motion. Therefore, this constant is directly related to changes in morphology.¹⁷ As a result, when the morphology changes, it causes changes in B, which results in modifications in the ionic conductivity. A previous study in which silk fibroin separators were prepared showed data to suggest that higher β -sheet content is correlated with higher ionic conductivity.²² Therefore, here we investigate how the ionic conductivity of silk/cellulose biocomposites varies according to a change in the structural and morphological properties within the films

In this study, 1-ethyl-3-methylimidazolium acetate (EMIMAc) and 1-ethyl-3-methylimidazolium chloride (EMIMCI) ionic liquids are used to dissolve the silk and cellulose biomaterials, which are then regenerated with aqueous solutions of either 25% hydrogen peroxide or 25% ethanol. The use of two different ionic liquids allows for a comparison of ionic conductivities based on changing just the anion in the ionic liquid structure. This small difference leads to morphological, thermal, mechanical and electrical property variations. Also, morphological changes, as well as ionic conductivity modifications, are seen between the two coagulation agents. The focus of this study was to determine how the formation of β -sheet and cellulose crystallinity, induced by the fabrication method, dictates changes in the ionic conductivity of a 50% silk, 50% cellulose film.

EXPERIMENTAL

Materials

Ionic liquid

EMIMAc (95%) and EMIMCI (98%) were both purchased from Sigma-Aldrich, St. Louis, MO, USA. The ionic liquids were pretreated by placing them in a vacuum oven (30 inHg) at 70 °C for 24 h to remove any water in the liquid.

Cellulose

Avicel microcrystalline cellulose of $250 \,\mu m$ (Techware Z26578-0) was acquired from Analtech. Before using the cellulose, it was placed in a vacuum oven (30 inHg) at 70 °C for 24 h.

Sill

Bombyx mori silk cocoons were purchased from Treenway Silks (Lakewood, CO, USA). The silkworm cocoons were boiled in a 0.02 mol L⁻¹ NaHCO₃ solution (Sigma-Aldrich) for 15 min to remove the sericin coating on the fibers. Deionized water was used to thoroughly rinse the cocoon fibers three times to ensure the sericin was entirely removed. The degummed fibers were air dried overnight and then put into a vacuum oven (30 inHg) at room temperature. This removed moisture on the surface of the fibers.

Dissolution of the protein and polysaccharide

The protein (silk) and polysaccharide (cellulose) were measured to make up 10% by mass of the biocomposite film, while the ionic liquid was measured to make up the remaining 90% by mass. The 10% solid mass of the film was broken down so that silk and cellulose would each account for 50% by mass. The two pretreated ionic liquids were measured into individual vials and placed in a silica oil bath on a hot plate at 80 °C. The bath was used to ensure that there was an even amount of heat distributed to the vials. The silk was first added to the vial followed by the cellulose once silk dissolution was complete. When the dissolution of both silk and cellulose was completed for each ionic liquid, the solution was allowed to mix for 24 h on the hot plate at the designated temperature.

Preparation of regenerated biofilm

The gel solution formed from the dissolution was transferred, after 24 h, to 3D printed molds made of ABS (Acrylonitrile butadiene



styrene) with dimensions of $12 \times 12 \times 1$ mm. Heated to 75 °C, 1 mL micropipette tips were used when pipetting the solution into the molds to ensure the solution did not solidify when transferring from vial to mold. The molds were placed in a 250 mL beaker filled with 100 mL of coagulation agent and sealed with Parafilm for 48 h to regenerate the materials and remove as much ionic liquid as possible from the film. After 48 h, the molds were removed, rinsed three times with distilled water to ensure removal of residual ionic liquid and transferred to a Teflon Petri dish. Then, the films were placed in a low-pressure desiccator under 4 inHg of vacuum for 72 h to allow drying.

Characterization

Scanning electron microscope

SEM was performed using a JEOL JCM-6000 scanning electron microscope, and images obtained from this were used to determine the topography of the films. Images were acquired at a magnification of 200× and are presented with a scale bar of 100 μm . The films were approximately 5 mm in width and were put into a Denton Desk II Au–Pd sputter coater to deposit a conductive film on the sample that mitigated the buildup of surface charge. Deposition took place for 60 s once the system pressurized and stabilized to 75 mTorr. This resulted in an Au–Pd coating 200 μm thick. After the samples were coated and drying of this Au–Pd coating was complete, they were ready for imaging.

Fourier transform infrared spectroscopy

Bruker's ALPHA-Platinum ATR-FTIR spectrometer with platinumdiamond sample module was used to perform the FTIR analysis. 4000 cm⁻¹ to 400 cm⁻¹ was the spectral range used to collect the data of the films. 128 background scans were performed along with 32 sample scans in six different locations of the film. Acetone was used to clean the FTIR diamond and hammer before the background scans were run as well as between each sample. Fourier self-deconvolution was used to study the amide I region $(1595-1705 \, \text{cm}^{-1})$. The Lorentzian line shape, with a 25.614 $\, \text{cm}^{-1}$ half-bandwidth and a noise reduction factor of 0.3, was used for performing deconvolution. Gaussian profiles were utilized to allow for fitting results and then integrated to find the area relating to a specific wavelength. All analyses were performed using Opus 7.2 software. The data were normalized from 4000 cm⁻¹ to 400 cm⁻¹ using mix-max normalization. This was used to better show functional groups in the spectra.

Thermogravimetric analysis

TGA was performed using the TA Instruments Discovery TGA system with 5 mg samples. All samples were under a nitrogen gas purge of 25 mL min⁻¹ and started at 30 °C. They underwent an isothermal period of 1 min and were then ramped at 10 °C min⁻¹ to 600 °C. Between each run, the furnace was cooled to 30 °C. Step transition analyses and derivative plots were utilized to determine the onset of decomposition ($T_{\rm onset}$), the weight-loss percentage of the sample and the temperature that corresponds to the decomposition of the sample at the highest rate ($T_{\Delta \rm Max}$).

Differential scanning calorimetry

A TA Instruments differential scanning calorimeter equipped with a refrigerated cooling system under a nitrogen gas flow of 50 mL min⁻¹ was utilized to analyze 5 mg samples contained in an aluminium Tzero pan. The DSC calibration was performed with

indium for heat flow and temperature. The DSC measurements were taken at an equilibration of room temperature, isothermal for 10 min, ramp 10.00 °C min⁻¹ to 120 °C, isothermal for 10 min to remove bound solvents, ramp 10.00 °C min⁻¹ back to -30 °C, isothermal for another 10 min, and ramp 10.00 °C min⁻¹ to 300 °C. Calibration of the heat flow and heat capacity were performed using aluminium and sapphire references.

X-ray scattering

X-ray scattering was performed with the multi-angle X-ray scattering system (DEXS) at the University of Pennsylvania at room temperature and under vacuum. The Xeuss 2.0 by Xenocs has a Cu X-ray source, computer controlled focusing and transmission incident sample geometries, a 1M pixel Pilatus detector (2D) and a smaller detector for simultaneous small angle (SAXS) and wide angle (WAXS) X-ray scattering. A full flux collimation was used with a slot of 1.2 mm \times 1.2 mm. Each sample was run for 200 s. For WAXS the beamstop was set at 160 mm and for SAXS at 350 mm which gave a scattering vector resolution from 1.1 to 3.1 nm⁻¹ and from 0.065 to 2.95 nm⁻¹, respectively. The intensity reported is not absolute intensity and thus is reported in arbitrary units (a.u.). All samples were dried in a vacuum for 24 h and subsequently cut into squares to span across the sample holder before X-ray scattering characterization. The X-ray scattering profiles were evaluated using Foxtrot 3.4.9; the isotropic 2D scattering patterns were azimuthally integrated to yield intensity versus scattering vector.

Atomic force microscopy (nanoindentation)

The elasticity and hardness of the silk/cellulose biocomposites were investigated by AFM-based nanoindentation. Samples were adhered to microscope slides by the sparse application of a cyanoacrylate-based adhesive and left to dry in a fume hood to mitigate settling of the adhesive vapor onto the sample surface. Prior to mounting the samples in the Asylum Research MFP-3D atomic force microscope, they were kept in a dehydrated state via storage in a vacuum desiccator. Nanoindentation was performed under ambient conditions using spherical indenters of radius 40 nm (Nanotools Biosphere B40-FM). The inverse optical lever sensitivity and spring constant of the cantilevers were calibrated using the microscope slide as an infinitely hard surface. This allows for an accurate relationship between cantilever deflection and the force applied by the indenter to the sample. A topological map was scanned over a $20 \,\mu\text{m} \times 20 \,\mu\text{m}$ area, and 25 load - displacement curves were recorded for each sample. In order to account for the adhesive forces between the indenter and the biocomposite, the Johnson - Kendall - Roberts (JKR) model was used to extract both the elastic modulus and hardness. The JKR approach is a modification of the Hertzian model that takes into account the attractive forces between the indenter and the sample surface.²³ It is regarded as a more accurate model when measuring soft materials where adhesion can have a stronger influence on the as-determined elasticity values.²⁴ Notbohm et al. state that the JKR model is more appropriately applied to the loading curve, as opposed to the unloading, when nanoindentation is performed in an AFM-based system.²⁵

Dielectric relaxation spectroscopy

The ionic conductivity of the biocomposites made with different ionic liquids and coagulation agents was measured using dielectric relaxation spectroscopy at the University of Pennsylvania. The Solartron Modulab XM materials test system was employed in the



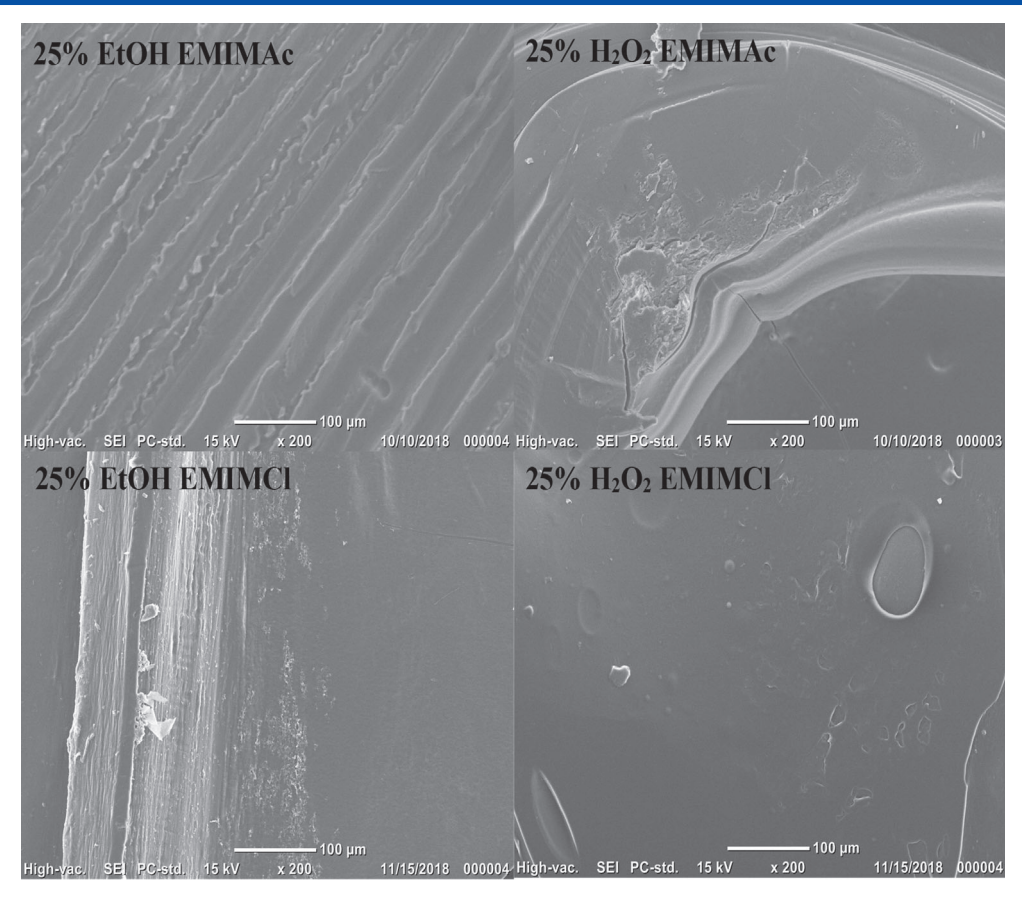


Figure 1. SEM images of regenerated films using various ionic liquids and coagulation agents.

frequency range 0.1 Hz to 1 MHz, and the samples were tested in the temperature range $300-450\,\mathrm{K}$ ($26.85-176.85\,^\circ\mathrm{C}$). The film was placed between two stainless steel electrodes, with the top plate having a diameter of 6 mm. When conductivity measurements were being taken, the sample was in a Janis VPF-100 cryostat under vacuum. ²⁶ The measurements began at a temperature of $450\,\mathrm{K}$ ($176.85\,^\circ\mathrm{C}$) to ensure no excess water was left in the sample, and the temperature was then decreased by $10\,\mathrm{K}$ for each measurement.

RESULTS AND DISCUSSION

The quantitative and qualitative data obtained from varying coagulation agents and ionic liquids while keeping the biomaterial compositions constant show morphological, thermal and mechanical property changes, as well as changes in ionic conductivity. Films regenerated using hydrogen peroxide were more brittle than those regenerated with ethanol. These distinct differences in morphology ultimately correlated with changes in the ionic conductivity of the biocomposite films. The following characterization tests provide more details about how varying the type of ionic liquid and coagulation agent causes changes in the structural, morphological, thermal and mechanical properties.

Scanning electron microscopy

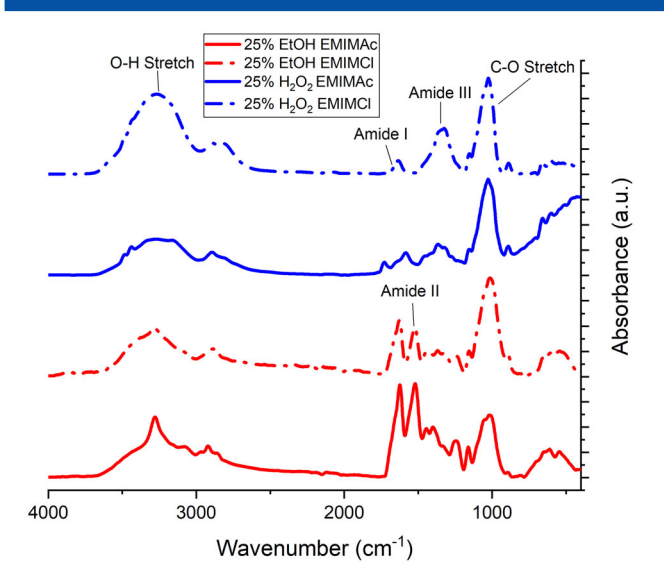
SEM was employed to examine the morphological and topographical properties of the regenerated silk/cellulose films, as seen in Fig. 1. All the films synthesized using different ionic

liquids and coagulation agents look different at the surface level. The EMIMAc film regenerated with ethanol has ridges running through the entire surface of the film. This differs from all the other films which do not have this distinct characteristic. The EMIMCI film regenerated with ethanol is relatively smooth with one larger ridge running down the middle of the entire film's surface. The films regenerated with hydrogen peroxide both seem to have a few shallow spheres on the surface. Specifically, the EMIMAc hydrogen peroxide film has one shallow sphere and has longer ridges running over almost the entire surface of the film. This differs from the EMIMCI hydrogen peroxide film which is much smoother than the EMIMAc hydrogen peroxide film. There are only a few shallow spheres on the surface, but surrounding areas are devoid of any large ridges like the rest of the films. From these images, it is possible to see the effect of various ionic liquids and coagulation agents on the topology of the various films.

Infrared spectroscopy

FTIR was used to ensure proper blending of the materials, as well as to calculate the secondary protein structures within the regenerated materials, as seen in Fig. 2. The IR spectra were normalized to compare peak sharpness and location for the various samples. In all of the spectra, the O-H group can be seen from approximately 3550 to 3000 cm⁻¹. The hydrogen peroxide films show this peak as being rounder than the ethanol films which show a sharp point. The peak can come from the O-H groups of cellulose as well as any leftover coagulation agent. The next peak seen in all the spectra is at approximately 2900 cm⁻¹. This corresponds to a C-H stretch seen in cellulose. Amide regions I, II and





 $\textbf{Figure 2.} \ FIIR \ spectra \ of the 50\% \ silk \ and 50\% \ cellulose \ regenerated \ films \ using \ various \ ionic \ liquids \ and \ coagulation \ agents.$

Ill are present in most biocomposites, which suggests that the silk is indeed present. These regions have similar wavenumbers in the films treated with ethanol and the films treated with hydrogen peroxide. However, the amide II region is missing from the EMIMCI film regenerated with hydrogen peroxide. The large main peak seen at approximately $1030~\rm cm^{-1}$ corresponds to the C–O stretch in cellulose. The small shoulder peak at approximately $1160~\rm cm^{-1}$ corresponds to the C–N stretch from the imidazolium ring in the ionic liquid. The low absorption of this C–N stretch peak possibly indicates that a minimal amount of ionic liquid remains in the films after using the coagulation agent.

Fourier self-deconvolution was used to analyze the amide I region from 1720 cm⁻¹ to 1590 cm⁻¹,²⁷ and the secondary structure content is summarized in Table 1. The side chains in all samples vary by a maximum of 5.9%. The hydrogen peroxide films do not differ at all since both have no side chains in the biocomposite films, whereas the ethanol films differ by 4.0% between ionic liquids. Turns have nearly the same value for ethanol samples but vary more in hydrogen peroxide films. There is only a 2.4% difference in turns for films coagulated with ethanol, whereas the hydrogen peroxide films vary by 11.1% with the EMIMAc films having a greater amount of turns. Random coils are more consistent with the ethanol coagulation agent compared to the hydrogen peroxide coagulation agent. Specifically, the ethanol films vary by 5.2% compared to the hydrogen peroxide films which vary by 9.3%. When looking at α -helices, ethanol samples vary less between ionic liquids than hydrogen peroxide films again. Specifically, samples made with EMIMCI have a 1.6% greater number of α -helices than EMIMAc samples. Conversely, hydrogen peroxide films vary

more between ionic liquids, specifically 13.6%. The EMIMAc hydrogen peroxide film has 11.6% more α -helices than the EMIMAC ethanol film. The EMIMCI hydrogen peroxide film has 3.6% fewer α -helices than the EMIMCI ethanol film. This shows that there is a difference not only between ionic liquids but also between coagulation agents. Finally, the β -sheet content differs between samples and is connected to the ionic conductivity, discussed later. The β -sheet content for hydrogen peroxide samples is exceptionally different, with the EMIMCI film having 34.2% more β -sheets than the EMIMAc film. This is different from both ethanol films, which do not differ vastly. There is only a 5.2% difference in β -sheet content, with the EMIMCI sample having a higher percentage than EMIMAc. Overall, the EMIMCI hydrogen peroxide sample has the highest β -sheet content of the three samples.

Thermogravimetric analysis

Figure 3 shows the thermograms obtained from TGA of the four different biocomposite films. In contrast, Fig. 4 shows the derivate weight-loss percentage thermograms, which help determine the maximum temperature of decomposition. These thermograms were used to determine the onset and end temperatures, as well as the weight-loss percentage and $T_{\Delta \mathrm{Max}}$. Table 2 displays the resulting values of the analyses using both of these figures. The films made using EMIMAc demonstrate a bimodal thermogram compared to the EMIMCI films. In this case, the biocomposites generated with EMIMCI show fewer interfaces than the samples made with EMIMAc. Previously, it was discussed that the bimodal result compared to pure material is strongly related to the number of interfaces formed during the mixing process.⁶ Looking at the thermograms, differences are also seen in the onset, end and $T_{\Lambda Max}$ temperatures. The difference between the onset temperatures for the hydrogen peroxide films varied by 38.5 °C. This is a slightly smaller difference compared to the ethanol films, which differed by 49.4 °C. The onset temperature for the EMIMAc ionic liquid was highest in the hydrogen peroxide sample, while the EMIMCI ionic liquid had the greatest onset temperature for the ethanol film. The onset temperature of the ethanol film in EMIMCI is approximately 15.0 °C higher than that for the hydrogen peroxide film in EMI-MAc. The ethanol film also has a higher percentage of β -sheets than the hydrogen peroxide film, about 32%, which could increase the onset temperature of the film. Again, the end temperature for EMIMAc coagulated with hydrogen peroxide is higher than that of the EMIMAc coagulated with ethanol by 14.1 °C. However, EMIMCI coagulated with hydrogen peroxide has a lower end temperature than EMIMCI coagulated with ethanol by 12.4 °C. This difference is slightly smaller than the difference in end temperatures between the EMIMAc films. When looking at the weight-loss percentage of the samples, the EMIMCI sample coagulated with ethanol had one of the lowest weight-loss percentages of 46.7%, only 1.7% greater than the EMIMCI sample coagulated with hydrogen peroxide. The EMIMCI ethanol film also corresponds to the highest onset temperature. Both samples using EMIMAc show a greater difference

Table 1. Secondary structure contents of 50% silk and 50% cellulose biocomposites						
Composition	Coagulation	Side chains	β -sheets	Random coils	lpha-helices	Turns
50/50 silk/cellulose from EMIMAc	25% H ₂ O ₂	0.0%	14.3%	39.8%	21.2%	24.6%
50/50 silk/cellulose from EMIMCI	$25\% H_2O_2$	0.0%	48.5%	30.5%	7.6%	13.5%
50/50 silk/cellulose from EMIMAc	25% EtOH	5.9%	41.0%	20.5%	9.6%	23.0%
50/50 silk/cellulose from EMIMCI	25% EtOH	1.9%	46.2%	15.3%	11.2%	25.4%



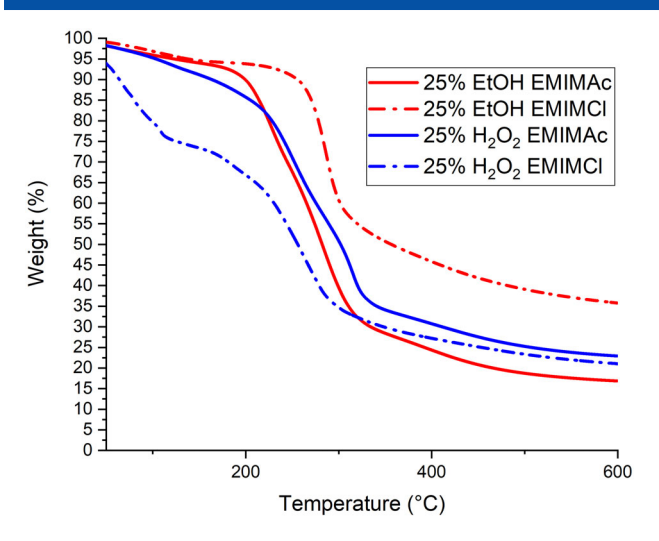


Figure 3. Thermograms of different silk/cellulose biocomposites.

in weight-loss percentage than the EMIMCI films which show relatively similar weight-loss percentages, with the film coagulated with ethanol only having 1.7% more weight loss than that of the hydrogen peroxide film. The hydrogen peroxide films showed an 11.0% difference in weight loss from the EMIMAc film to the EMIMCI film. This is different from the ethanol films which showed a greater difference in the weight-loss percentage. Specifically, the EMIMAc film coagulated with ethanol lost 20.6% more of its weight than the EMIMCI sample. The $T_{\Delta \text{Max}}$ is highest for the EMIMAc film coagulated with hydrogen peroxide, while the lowest value corresponds to the EMIMCI film coagulated with hydrogen peroxide. There is very little difference between the ethanol samples, 2.1 °C, while the hydrogen peroxide films vary by 50.2 °C, a much more significant difference than the ethanol films. It is also interesting to note that the EMIMCI film coagulated with hydrogen peroxide had more water retention than all the other samples. These results show how much the anion of the ionic liquid as well as the coagulation agent can affect the thermal stability of the silk/cellulose biocomposites.

Differential scanning calorimetry

Figure 5 shows standard DSC scans for the four different samples of biocomposites using ethanol, hydrogen peroxide, EMIMAc and EMIMCI as coagulation agents and ionic liquids respectively. The EMIMAc hydrogen peroxide sample has a crystallization peak at approximately 537 K (263.85 °C) while the EMIMCI hydrogen peroxide sample has a crystallization peak at approximately 523 K (249.85 °C), 14 K lower. The film prepared using EMIMCI has a much more defined, sharp crystallization peak compared to the film made with EMIMAc. The same is true of the films coagulated with ethanol. The EMIMCI film coagulated with ethanol has a sharp

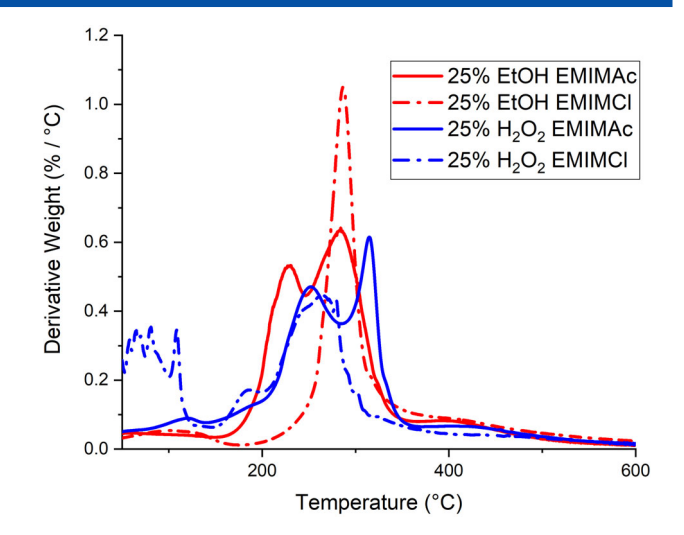


Figure 4. Derivative weight-loss percentage plots of the biocomposite films used to determine $T_{\Delta \rm Max}$.

crystallization peak at approximately 552 K (278.85 °C), higher than both hydrogen peroxide samples as well as the other ethanol film. The EMIMAc film coagulated with ethanol seems to have two crystallization peaks, with the peak at the highest temperature being 515 K (241.85 °C). This is lower than all other samples. This sample also seems to have an endothermic peak at approximately 542 K (268.85 °C). This peak could correspond to additional interface loss in the sample after the first two crystallization peaks. The DSC graphs were also analyzed to determine the glass transition temperatures of the films, as seen in Table 3. Samples coagulated with hydrogen peroxide had much lower glass transition temperatures than those coagulated with ethanol. Specifically, the EMIMAc sample coagulated with hydrogen peroxide had a temperature 60.7 K lower than that of the EMIMAc sample coagulated with ethanol. Similarly, the EMIMCI sample coagulated with hydrogen peroxide had a temperature 98.9 K lower than that of the EMIMCI sample coagulated with ethanol. It is also possible to see that films created using ethanol varied less between samples than the hydrogen peroxide films. Ethanol films only vary by 9.5 K, with the EMIMCI film having a higher glass transition temperature. This is different from the hydrogen peroxide samples which vary by 28.7 K, and the EMIMAc film has a higher glass transition temperature. In this case, the hydrogen peroxide, as coagulation agent, affected the material crystallinity but it also affected the formation of silk secondary structures such as the β -sheet content and the random coil content, as demonstrated in the FTIR section. We believe that the protein secondary structure interactions in conjunction with the cellulose amorphous regions increase the segmental motion of the biocomposite thus reducing the glass transition temperature. These glass transition temperatures are

Table 2.	Start and end temperatures, total weight-loss percentage and the maximum temperature of the derivative representing when maximum
weight lo	ss occurred are used to characterize the TGA results

Composition	Coagulation	$T_{ m onset}$ (°C)	$T_{\rm end}$ (°C)	Weight loss (%)	$T_{\Delta Max}$ (°C)
50/50 silk/cellulose from EMIMAc	25% H ₂ O ₂	251.1	325.7	56.0	314.7
50/50 silk/cellulose from EMIMCI	25% H ₂ O ₂	212.6	290.2	45.0	264.5
50/50 silk/cellulose from EMIMAc	25% EtOH	216.7	311.6	67.3	284.2
50/50 silk/cellulose from EMIMCI	25% EtOH	266.1	302.6	46.7	286.3



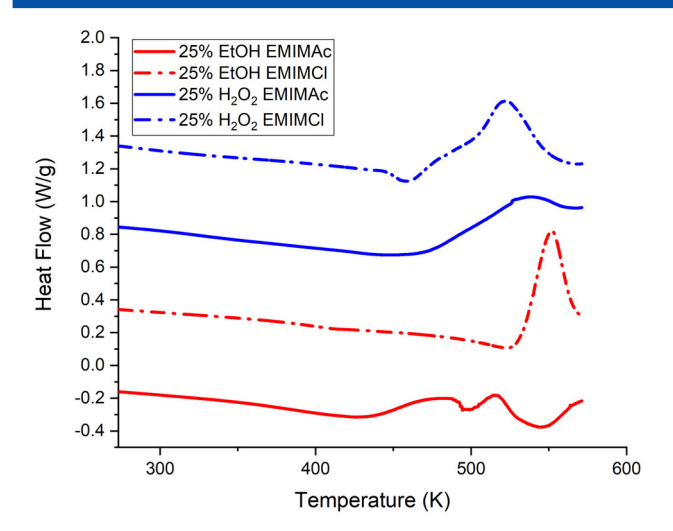


Figure 5. DSC heat flow scans of the silk/cellulose biocomposite films used to determine the glass transition temperatures.

Table 3. Glass transition temperatures of films created using various ionic liquids and coagulation agents, determined by DSC (in °C and K) Composition Coagulation T_{g} (°C) $T_{\alpha}(K)$ 50/50 silk/cellulose from EMIMAc 56.3 329.4 25% H₂O₂ 50/50 silk/cellulose from EMIMCI 25% H₂O₂ 300.7 27.6 50/50 silk/cellulose from EMIMAc 25% EtOH 390.1 117.0 50/50 silk/cellulose from EMIMCI 25% EtOH 126.5 399.6

later used to normalize the ionic conductivity data that were collected.

X-ray scattering

The morphological investigation was initiated by looking at the distinct spacing observed in the pure materials (e.g. silk fiber and cellulose powder).5 For the silk fibers in Fig. 6, six scattering peaks are observed moving from high to low scattering vector regions. The peaks are located at $q_1 = 1.34 \,\mathrm{nm}^{-1}$, $q_2 = 6.53 \,\mathrm{nm}^{-1}$, $q_3 = 14.80 \, \text{nm}^{-1}$ $q_4 = 17.60 \, \text{nm}^{-1}$ $q_5 = 23.46 \, \text{nm}^{-1}$ $q_6 = 28.88 \,\mathrm{nm}^{-1}$. The d-spacings for each peak are calculated by using the $d = 2\pi/q$ formula and are $d_1 = 4.69$ nm, $d_2 = 0.96$ nm, $d_3 = 0.42 \text{ nm}$ $d_4 = 0.36 \text{ nm}$, $d_5 = 0.27 \text{ nm}$ and $d_6 = 0.22 \text{ nm}$, respectively. The d-spacings observed at 0.42, 0.36, 0.27 and 0.22 nm correspond to the distance between β -strands and the primary structure, in particular the silk II crystalline spacings, the distance at 0.96 nm corresponds to the inter-sheet distance between β -sheets and the distance at 4.69 nm corresponds to the size of the β -sheets in the lateral direction. ^{28–34} In cellulose powder, three distinct spacings are observed. The microfibril distance is related to crystal size, $q_1 = 1.75 \,\mathrm{nm}^{-1}$ (3.58 nm). The other spacings in cellulose can be attributed to its monoclinic unit cell of cellulose I_{β} equatorial lattice planes ($q_2 = 16.10 \text{ nm}^{-1}$ and $q_3 = 10.90 \,\mathrm{nm}^{-1}$). Between q_1 and q_2 , there are two small peaks at $q_a = 14.29 \,\mathrm{nm}^{-1}$ and $q_b = 12.42 \,\mathrm{nm}^{-1}$. The calculated d-spacings are $d_2 = 0.39 \,\text{nm}$, $d_3 = 0.57 \,\text{nm}$, $d_a = 0.44 \,\text{nm}$ and $d_b = 0.50 \,\text{nm}$. The other scattering peaks ($q_4 = 20.75 \text{ nm}^{-1}$, $q_5 = 24.71 \text{ nm}^{-1}$ and $q_6 = 29.67 \text{ nm}^{-1}$) are related to the cellulose crystallinity spacings. In support of the data, Vainio et al. reported the crystalline monoclinic cellulose of Avicel with a scattering vector and reflection

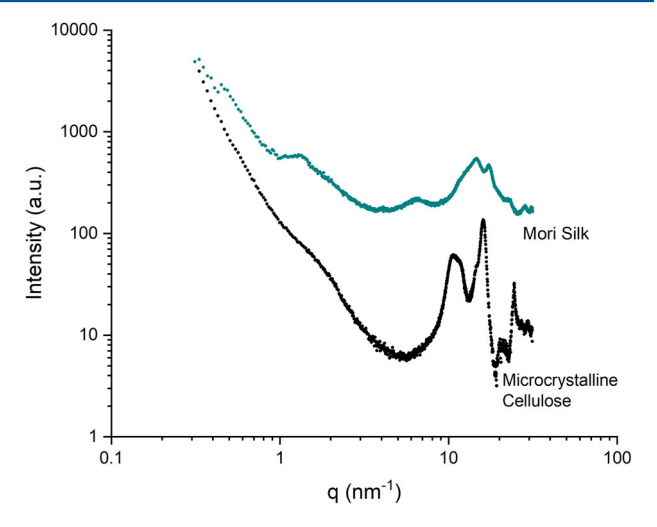
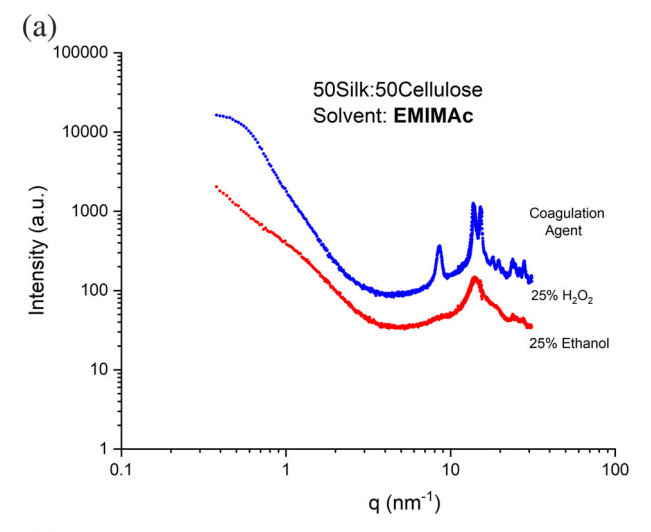


Figure 6. X-ray scattering profiles for Mori silk and microcrystalline cellulose.

values of 15.7 nm⁻¹ (200), 11.84 nm⁻¹ (110) and 10.5 nm⁻¹ (110).³⁵ The 0.6 nm index is related to the longer side of the square structure which is always parallel to a side of the crystal. Helbert *et al.* suggest that the cellulose microfibrils could be the packing of several sheets of the 0.6 nm lattices.⁹ The crystal size estimation for Avicel using the Scherrer equation is 3.97 nm, which matches published data of related systems.^{36–40}

The scattering profile for the silk/cellulose biocomposites is shown in Fig. 7. The 2D scattering profiles (not shown here) showed isotropic rings for all biocomposites. Independent of the type of ionic liquid used as solvent, the data show that the films coagulated with hydrogen peroxide are more semicrystalline than the samples coagulated with ethanol. The semicrystalline regions of the sharp peak are associated with the regions of cellulose rather than silk. To demonstrate this effect, 100% cellulose films were regenerated using EMIMAc as the solvent and coagulated with hydrogen peroxide and ethanol. Figure 8 shows the X-ray scattering profile for these two samples. As the X-ray scattering profile demonstrates, hydrogen peroxide increases the cellulose crystallinity while ethanol does not affect the crystallinity. A coagulation agent in the form of an alcohol induces changes in the protein β -sheet formation as previously demonstrated.⁴¹ In continuation with the silk/cellulose biocomposites, attention is attracted to the morphological effect as a function of coagulation agent and type of ionic liquid with various correlation distances. The peak position, scattering vector (q) and d-spacing calculated using the $d = 2\pi/q$ formula are reported in Tables 4 and 5. Peak 1 represents the minimum scattering vector observed in the X-ray scattering. This peak was observed in both biocomposites which were coagulated with EMIMAc, independent of coagulation agent; however, it is dependent on the type of ionic liquid. Interestingly, the d-spacing increases from 5.28 to 13.4 nm as the coagulation agent changes from ethanol to hydrogen peroxide. This peak is related to the average microfibril cross-sectional dimension⁵ and is dependent on the composition of the materials and type of ionic liquid, as previously published.⁴ The diameter of the microfibrils is known to range from about 2 to 20 nm. 42 Peak 2 is indicative of the existence of an intercalation structure with the insertion of either silk into cellulose or cellulose into silk.⁵ This peak intensity increases with hydrogen peroxide; however, the d-spacing remains constant, independent of solvent and coagulation agent, at an average of





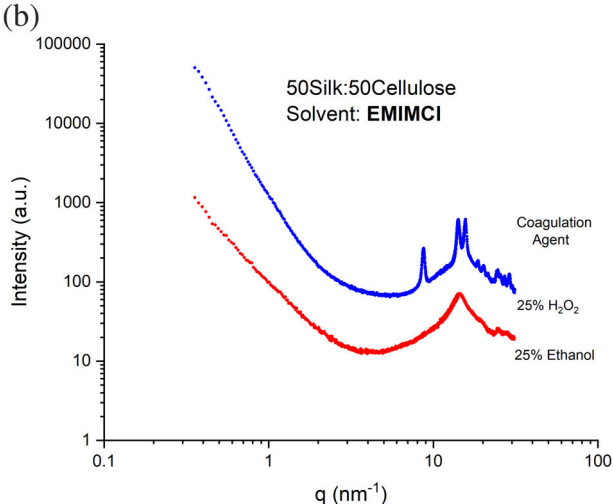


Figure 7. X-ray scattering profiles for silk/cellulose biocomposites as a function of coagulation agent and ionic liquid type.

0.73 nm. In pure silk, this region is related to the distance between β -sheets. It is now possible to confirm that the cellulose strands can directly affect its formation. Peaks 3 and 4 are attributed to the cellulose unit cell spacing and to the distance between silk β -strands which depend on solvent and coagulation agent. This region includes the silk I spacing which is a mixture of α -helices, β -sheets and random coils. In Tables 4 and 5, it can be seen that the samples regenerated with EMIMAc have slightly higher spacing than those regenerated with EMIMCI. This is due to intermolecular and intramolecular interactions between the acetate anion oxygen receptors and the hydroxide groups in natural fibers and in cellulose molecules which are greater than the chloride ion. This is important because it is now possible to suggest that backbone to backbone spacing between molecules is affected by the type of anion in the ionic liquid solvent. Peaks 5 to 15 are related to the crystalline periodicity of cellulose, but also include correlation distances from the silk II structures as previously shown in Fig. 6.

In summary, the X-ray scattering profiles show a semicrystalline structure for all samples coagulated with hydrogen peroxide which is independent of solvent type. It can be confirmed that the level of disruption of β -sheet formation and cellulose microfibrils can be affected by the type of ionic liquid. The various results demonstrate that intermolecular and intramolecular interactions

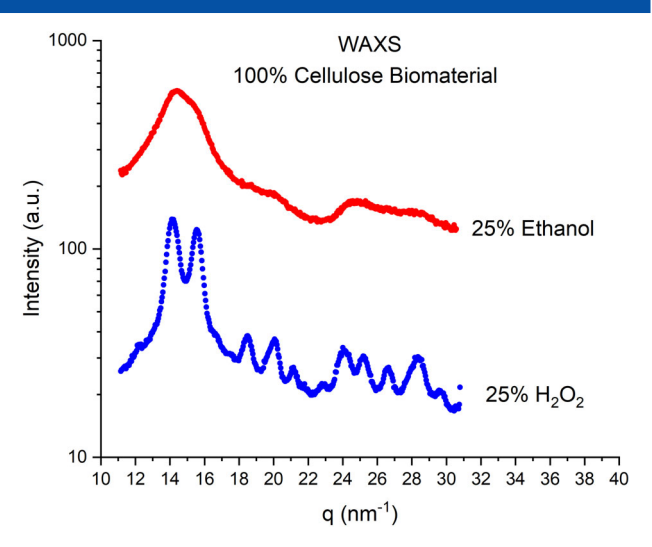


Figure 8. X-ray scattering profiles for 100% cellulose films as a function of coagulation agent.

Table 4. Scattering vector and correlation distances for silk/cellulose biocomposites dissolved in EMIMAc and coagulated with two different coagulation agents

	EMIMAc, q (nm ⁻¹)/ d (nm)		
Peak position	H ₂ O ₂	Ethanol	
1	0.47/13.4	1.19/5.28	
2	8.6/0.73	8.6/0.73	
3	13.8/0.46	14.2/0.44	
4	15.3/0.41	-	
5	16.4/0.38	-	
6	18.1/0.35	19.3/0.32	
7	19.7/0.32	-	
8	20.7/0.30	-	
9	21.6/0.29	-	
10	22.4/0.28	23.9/0.26	
11	23.9/0.26	-	
12	24.8/0.25	-	
13	26.2/0.24	-	
14	28.0/0.22	27.8/0.22	
15	29.4/0.21	-	

between the silk and cellulose molecules can be controlled with the type of coagulation agent which causes changes in the thermal, mechanical and ionic conductivity properties.

Atomic force microscopy (nanoindentation)

AFM-based nanoindentation was carried out on biocomposite samples formed by each of the four ionic liquid/coagulant combinations. The measured load – indentation curves were fitted to the JKR model by way of the analysis tool accompanying the Asylum MFP-3D software package (v31). Maximum indentation depth was on average 30 nm, where only the initial 10 nm was fitted in order to avoid nonlinearities. As seen in Fig. 9, the use of hydrogen peroxide in place of ethanol results in a significant (*t* test, 0.35) increase in the elastic modulus from 54 to 139 MPa for EMIMAC; in the case of EMIMCI, the observable increase is far less significant (*t* test, 0.064) with a change from 178 to 199 MPa. The sample hardness follows a similar trend where hydrogen peroxide results



Table 5. Scattering vector and correlation distances for silk/cellulose biocomposites dissolved in EMIMCI and coagulated with two different coagulation agents

	EMIMCI, q (nm ⁻¹)/ d (nm)		
Peak position	H ₂ O ₂	Ethanol	
1	-	-	
2	8.8/0.71	_	
3	14.2/0.44	14.4/0.44	
4	15.8/0.40	_	
5	16.8/0.37	_	
6	18.7/0.33	20.0/0.31	
7	20.2/0.31	_	
8	21.4/0.29	-	
9	23.2/0.27	_	
10	24.6/0.25	25.0/0.25	
11	25.7/0.24	_	
12	27.2/0.23	-	
13	29.00/0.22	_	
14	30.4/0.21	-	
15	31.2/0.20	-	

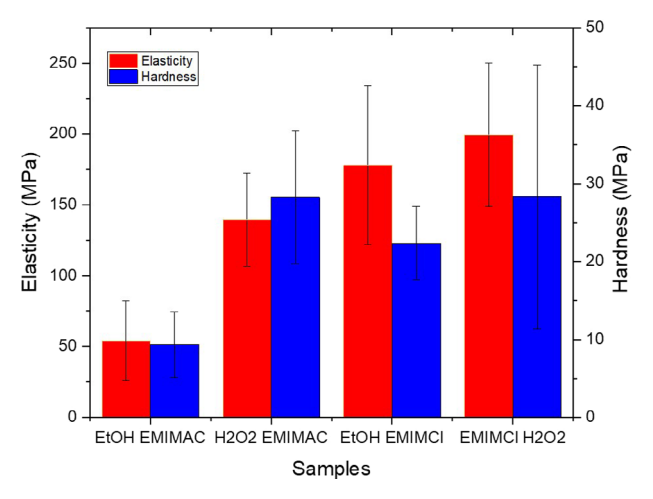


Figure 9. Elasticity and hardness for biocomposites as a function of coagulation agent and ionic liquid type.

in a large increase for EMIMAc. However, between ionic liquids, coagulation with hydrogen peroxide results in a similar hardness of 28 MPa. These data correlate with the X-ray scattering profiles shown above, where the degree of crystallinity was dependent on the coagulant (i.e. films regenerated with hydrogen peroxide are more semicrystalline) but independent of the ionic liquid.

Dielectric relaxation spectroscopy

Figure 10 shows the ionic conductivities of the biocomposite films calculated at various temperatures. The results are reported with 1000/T on the x-axis and the logarithm of the conductivity on the y-axis. In order to calculate the conductivity, the relationship $\sigma = L/AR$ was used, where A is the cross-sectional area of the polymer film and L is the distance between the two inner electrodes. R is the resistance calculated at each temperature using the Nyquist plot. The high x-intercept of the semicircle is equal to the resistance. Using all this information, the ionic conductivity is calculated at

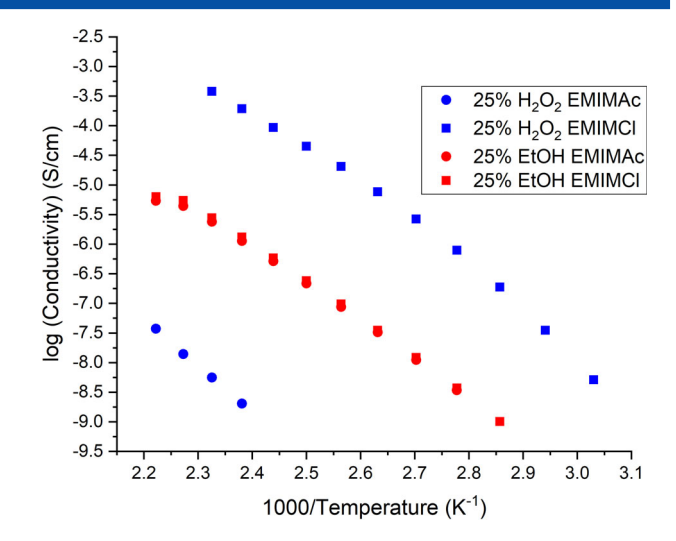


Figure 10. Ionic conductivity of the silk/cellulose biocomposites *versus* temperature.

each temperature. As shown in Fig. 10, the EMIMCI sample coagulated with hydrogen peroxide has the highest ionic conductivity, followed by the EMIMCI sample coagulated with ethanol, the EMIMAc sample coagulated with ethanol and finally the EMIMAc sample coagulated with hydrogen peroxide. It is important to note that the ionic conductivities of the films coagulated with ethanol are almost identical and collapse onto one line. The EMIMCI hydrogen peroxide sample has an ionic conductivity much higher than that of the EMIMAc hydrogen peroxide sample. This can be connected to the β -sheet content in the films. The EMIMCI sample has 48.5% β -sheets while the EMIMAc sample only has 14.3%. The higher β -sheet content corresponds to higher ionic conductivity of the sample. While the hydrogen peroxide samples differ in conductivity, the ethanol samples have nearly the same conductivity. Specifically, the EMIMCI ethanol sample has a slightly higher ionic conductivity than that of the EMIMAc ethanol sample. This can also be connected to the differences in the β -sheets. The EMIMCI ethanol sample has 46.2% β -sheets while the EMIMAc ethanol sample has 41.0% β -sheets. This small difference in β -sheets could change the ionic conductivity of the samples. Again, the sample with the higher β -sheet content has a higher ionic conductivity compared with the corresponding coagulation agent sample.

As shown in Fig. 11, the $T_{\rm q}$ -normalized ionic conductivity corrects for the segmental motion of the macromolecules making it possible to clearly demonstrate the effect of morphology. If all the data points had collapsed onto one curve or one line, the glass transition temperature would be the only contributing factor in the differences in ionic conductivity. However, since this did not occur, it is reasonable to assume that other factors are affecting the ionic conductivity, such as the morphology which will affect the differences in ion hopping or segmental motion of the polymer chains. 43,44 The samples coagulated with hydrogen peroxide, which have the highest cellulose crystallinity, have the lowest ionic conductivity. Curiously, the data suggest that the samples with the highest β -sheet content have a higher ionic conductivity independent of coagulation agent. The higher the β -sheet content is, the greater is the ionic conductivity. This type of phenomenon was observed in a recent publication by Lanceros-Méndez and colleagues.²² In that research, the ionic conductivity of silk fibroins increased with an increase in β -sheet content. The study also suggested that the β -sheets enhanced ion



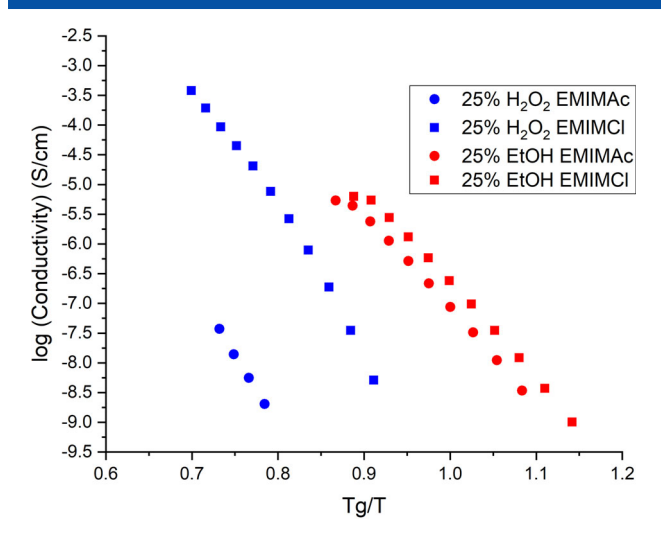


Figure 11. Ionic conductivity data normalized using the glass transition temperature.

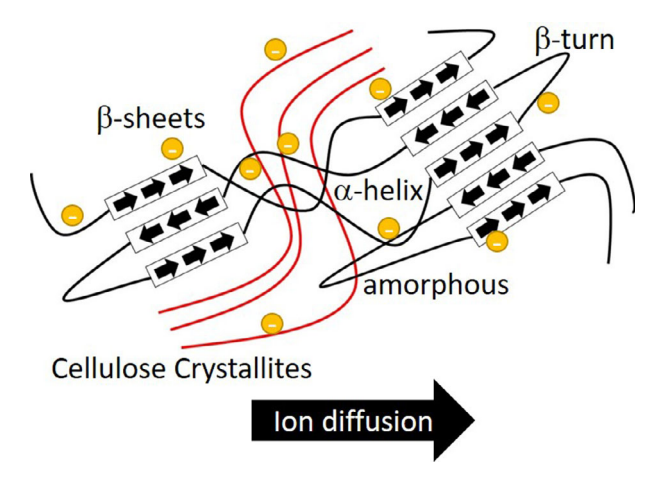


Figure 12. Schematic representation of ion diffusion in a solid electrolyte based on silk/cellulose biocomposites.

mobility. Considering these results, the data provide evidence to suggest a strong relationship between morphology and ionic conductivity; in particular, the relationship between cellulose crystallinity and silk β -sheet formation is shown to have a direct effect upon ionic conductivity. In the schematic representation in Fig. 12, ion diffusion is dependent on protein β -sheet size and orientation, and cellulose crystallinity. Since the cation concentration remains constant across the films, Fig. 12 also illustrates the chloride or acetate anions from the residual ionic liquid remaining in the film after the 48 h coagulation bath which are the source of ionic conduction in the film. Their interaction in the matrix will be affected by silk β -sheet content or by cellulose crystallinity. For the results, it is possible to conclude that β -sheets can enhance ionic conductivity.

CONCLUSION

Varying ionic liquids and coagulation agents of the silk/cellulose biocomposites altered the morphological, thermal, mechanical and ionic conductivity properties of the samples. The results of FTIR reveal distinct differences in secondary structures in the amide I region. Specifically, the EMIMCI sample coagulated

with hydrogen peroxide had the highest β -sheet content, followed by the ethanol samples, and finally the EMIMAc sample coagulated with hydrogen peroxide had the lowest β -sheet content. Measurement of thermal properties shows distinct differences between the various ionic liquids and coagulation agents. In terms of thermal stability, the EMIMCI sample coagulated with ethanol shows the highest onset temperature and one of the lowest weight-loss percentages. This connects to the glass transition temperatures obtained from DSC, where the EMIMCI ethanol sample exhibits the highest transition temperature. Compared to the ethanol samples, the hydrogen peroxide films have much lower glass transition temperatures. Furthermore, the X-ray scattering showed that the samples coagulated with hydrogen peroxide are more semicrystalline than those coagulated with ethanol, and the morphology is independent of ionic liquid. The nanoindentation results also confirmed, by the mechanical properties, that the samples coagulated with hydrogen peroxide had the highest hardness. All these results ultimately correlate with the ionic conductivity of the biocomposite films. The ionic conductivity correlated to the β -sheet content. The EMIMCI hydrogen peroxide film had the highest ionic conductivity as well as the highest β -sheet content, followed by the EMIMCI and EMIMAc ethanol samples which had the next lowest β -sheet content, and the EMIMAc hydrogen peroxide sample having the lowest ionic conductivity along with the lowest β -sheet content. This work confirms what has been suggested by others - that higher β -sheet content leads to higher ionic conductivity.²² While further investigations will be needed to understand this phenomenon fully, this work shows that new biocomposite films in which the ionic conductivity can be tuned for specific needs are possible. This is particularly promising for the development of new technologies that utilize natural biomacromolecules as bio-electrolytes.

ACKNOWLEDGEMENT

We want to acknowledge the funding provided by the NSF-DMR-REU (1809354 and 1809541) and NSF-MRI-CMMI (0922946), Rutgers University - Camden Laboratory Start-up funds and the State of New Jersey ELF Grant to Rutgers-Chemistry. We want to thank the LRSM including Professor Karen Winey, Professor Paul Heiney, Dr Francisco Buitrago, Benjamin Paren and Lu Yan at the University of Pennsylvania for training with regard to the X-ray scattering equipment (DEXS) as well as the dielectric relaxation spectroscopy equipment. The DEXS is funded by NSF-MRSEC (17-20530), NSF-MRI (17-25969), ARO DURIP (W911NF-17-1-02822) and the University of Pennsylvania. Xiao Hu was also supported by the Rowan University Start-up Grants and NSF Materials Engineering and Processing program (CMMI-1561966). Bailey Blessing is funded by the Department of Chemistry TA Line and Stacy A. Love is funded by the Center for Computational and Integrative Biology TA Line from Rutgers Camden. Lastly, we want to acknowledge the funding by the NSF-DBI-1559868 for supporting Karleena Rybacki as a 2018 REU undergraduate student.

DATA INFORMATION

Upon publishing, all data and protocols are located in: https://figshare.com/projects/Morphology_and_ionic_conductivity_relationship_in_silk_cellulose_bio-composites/61109.





REFERENCES

- 1 Yin J and Luan S, Regener Biomater 3:129-135 (2016).
- 2 Pavlovic M, Bioengineering: A Conceptual Approach. Springer International Publishing, Switzerland (2015). https://www.springer.com/us/book/9783319107974
- 3 Jia X, Wang C, Zhao C, Ge Y and Wallace GG, *Adv Funct Mater* **26**:1454–1462 (2016).
- 4 Stanton J, Xue Y, Pandher P, Malek L, Brown T, Hu X et al., Int J Biol Macromol 108:333–341 (2018).
- 5 Stanton J, Xue Y, Waters JC, Lewis A, Cowan D, Hu X *et al.*, *Cellul* **24**:1775–1789 (2017).
- 6 Hadadi A, Whittaker JW, Verrill DE, Hu X, Larini L and Salas-de la Cruz D, Biomacromolecules 19:3970 – 3982 (2018).
- 7 Hu X, Cebe P, Weiss AS, Omenetto F and Kaplan DL, *Mater Today* 15:208–215 (2012).
- 8 Zhou L, Wang Q, Wen J, Chen X and Shao Z, *Polymer* **54**:5035–5042 (2013).
- 9 Helbert W, Nishiyama Y, Okano T and Sugiyama J, J Struct Biol 124:42-50 (1998).
- 10 Cheng G, Varanasi P, Li C, Liu H, Melnichenko YB, Simmons BA *et al.*, *Biomacromolecules* **12**:933–941 (2011).
- 11 Agarwal V, Huber GW, Conner WC Jr and Auerbach SM, J Chem Phys 135:10B605 (2011).
- 12 Dumitriu S ed, *Polysaccharides: Structural Diversity and Functional Versatility*, 2nd edn. CRC Press, Boca Raton, FL (2004). https://www.taylorfrancis.com/books/9780429131660
- 13 Zhang H, Wu J, Zhang J and He J, Macromolecules 38:8272–8277 (2005).
- 14 Johnson KE, Electrochem Soc Interface 16:38-41 (2007).
- 15 Pinkert A, Marsh KN, Pang S and Staiger MP, Chem Rev **109**:6712–6728 (2009).
- 16 Freddi G, Romanò M, Massafra MR and Tsukada M, J Appl Polym Sci 56:1537 – 1545 (1995).
- 17 Salas-de la Cruz D, Morphology and Ionic Conductivity of Polymerized Ionic Liquids. University of Pennsylvania, Philadelphia, PA, USA (2011).
- 18 Klein RJ, Zhang S, Dou S, Jones BH, Colby RH and Runt J, *J Chem Phys* **124**:144903 (2006).
- 19 Lee M, Choi UH, Colby RH and Gibson HW, *Chem Mater* **22**:5814–5822 (2010).
- 20 Lovrić M, J Solid State Electrochem 1:116-116 (1997).
- 21 Chen H, Choi J-H, Salas-de la Cruz D, Winey KI and Elabd YA, *Macro-molecules* 42:4809–4816 (2009).

- 22 Pereira RF, Brito-Pereira R, Gonçalves R, Silva MP, Costa CM, Silva MM et al., ACS App. Mater Interfaces 10:5385 5394 (2018).
- 23 Johnson KL, Kendall K and Roberts A, *Proc R Soc Lond A Math Phys Sci* 324:301–313 (1971).
- 24 Ebenstein DM and Pruitt LA, Nano Today 1:26-33 (2006).
- 25 Notbohm J, Poon B and Ravichandran G, J Mater Res 27:229–237 (2012).
- 26 Griffin PJ, Freyer JL, Han N, Geller N, Yin X, Gheewala CD et al., Macro-molecules 51:1681 1687 (2018).
- 27 Hu X, Kaplan D and Cebe P, Macromolecules 39:6161-6170 (2006).
- 28 Um IC, Kweon H, Park YH and Hudson S, Int J Biol Macromol 29:91 97 (2001).
- 29 He S-J, Valluzzi R and Gido SP, Int J Biol Macromol **24**:187 195 (1999).
- 30 Gong Z, Huang L, Yang Y, Chen X and Shao Z, Chem Commun 48:7506–7508 (2009).
- 31 Asakura T, Yamane T, Nakazawa Y, Kameda T and Ando K, *Biopolymers* **58**:521–525 (2001).
- 32 Asakura T, Okushita K and Williamson MP, *Macromolecules* **48**:2345–2357 (2015).
- 33 Liu X and Zhang K-Q, Silk Fiber Molecular Formation Mechanism, Structure-Property Relationship and Advanced Applications, Oligomerization of Chemical and Biological Compounds. IntechOpen (2014). DOI: 10.5772/57611. Available: https://www.intechopen.com/books/oligomerization-of-chemical-and-biological-compounds/silk-fiber-molecular-formation-mechanism-structure-property-relationship-and-advanced-application
- 34 Saitoh H, Ohshima K-i, Tsubouchi K, Takasu Y and Yamada H, *Int J Biol Macromol* **34**:259–265 (2004).
- 35 Vainio U, Maximova N, Hortling B, Laine J, Stenius P, Simola LK *et al.*, *Langmuir* **20**:9736–9744 (2004).
- 36 Nieduszynski I and Preston R, *Nature* **225**:273 274 (1970).
- 37 Eyley S and Thielemans W, Nanoscale **6**:7764–7779 (2014).
- 38 French AD, Cellul 21:885-896 (2014).
- 39 Fernandes AN, Thomas LH, Altaner CM, Callow P, Forsyth VT, Apperley DC et al., Proc Natl Acad Sci 108:E1195 – E1203 (2011).
- 40 Kafle K, Shin H, Lee CM, Park S and Kim SH, *Sci Rep* **5**:15102 (2015).
- 41 DeFrates K, Markiewicz T, Callaway K, Xue Y, Stanton J, Salas-de la Cruz D et al., Int J Biol Macromol **104**:919–928 (2017).
- 42 Kamel S, eXPRESS Polym Lett 1:546-575 (2007).
- 43 Salas-de la Cruz D, Green MD, Ye Y, Elabd YA, Long TE and Winey KI, J Polym Sci B 50:338–346 (2012).
- 44 Ye Y and Elabd YA, *Polymer* **52**:1309–1317 (2011).